AUTOMATION AND CONTROL IN A SUBMARINE DRILL RIG

AG Arriaga, M Devincenzi, N Pérez and A Deu
Igeotest, Figueres, Spain

M Arroyo
UPC, Barcelona, Spain

Abstract
Remotely operated submarine drills are gaining acceptance as offshore geotechnical investigation tools for they provide a more convenient and often cheaper solution to geotechnical drilling vessels. The MD500 is an underwater subsea geotechnical drilling rig developed by Igeotest with the goal of retrieving high-quality physical samples of the seabed at study depths of up to 150m and with a nominal water depth of 500m. Control and automation are two key aspects with strong impact in its operational performance and ease of use, for the machine is composed of a set of remotely operated devices that must synchronize with each other: drilling rig, stabilizing legs and three manipulators for handling sampling tubes and drilling tools. These manipulators can be operated in a semi-automated fashion to help the operator focus on the drilling task. Further benefits of drilling and handling task automation include reduction of cycle time and increased repeatability, which leads to higher efficiency rates and, thus, overall reduction of operation costs. This paper presents control and operations details of the equipment as well as results yielded by several operation tests and experiments.

1. Introduction

1.1 Offshore geotechnical survey modes

A very important consideration when planning an offshore geotechnical campaign is the high cost of the equipment needed to deploy and perform the survey. In shallow waters, geotechnical surveys are usually carried out from jack-up platforms directly supported on the bottom. For depths beyond 30m the requirements on these jack-ups quickly increase, making them unpractical for geotechnical surveys, except perhaps in the calmest seas.

The alternative is to use vessels. But, again, the size, type and cost of the vessel needed depend on the depth and methods used for sample retrieval. The main two methods (ISO19901-8) are:

- From drilling vessel (downhole mode – according to ISO19901-8 nomenclature), in which the testing and sampling are carried out from a ship through an assembly of drill pipes.
- Using remotely operated underwater machines (seabed mode – according to ISO19901-8 nomenclature), in which the rig is placed on the seabed and operated remotely.

In the downhole mode a specially designed vessel that includes a drilling rig compatible with the drilling and sampling elements is needed. These specialist ships are relatively big – 70m lengths are common- and expensive to deploy and maintain.

On the other hand for the seabed mode, remotely operated machines, usually have a size small enough to be stored in standard 6m containers and their weight ranges from 10 to 15 tons. Medium size vessels for geotechnical research of offshore platform supply, of which a larger pool is available, are generally enough to deploy these pieces of equipment, thus reducing a significant item in the cost of the campaign.

1.2 Submarine geotechnical drills

The idea of executing drilling operations on the seabed has been around for long (Tirey, 1972). However, the technology is complex and it was not until the 1990s that it had an upsurge in development, with a clear focus on geotechnical

engineering surveys rather than on oceanographic research.

The pioneering work in this respect was that leading to the PROD series of drills (Carter et al., 1999). These drills have been commercially operative for more than a decade (Pennington & Kelleher, 2007). Later developments include the Rovdrill series, (Spencer et al., 2011) and the MeBo series (Spagnoli & Freudenthal, 2013; Spagnoli et al., 2015).

These machines were all originally developed aiming for oceanographic and marine resource surveys in the deepest waters (above 2000m depth). In those conditions the advantages of seafloor-based drilling over vessel-based drilling are clear. However, as the water depth reduces, the operational advantage also reduces, and fixed-cost items like required operational specialist crew size become more important. One possible avenue to limit those costs is by taking profit of the enhanced possibilities for automation and advanced control inherent in remotely operated systems.

1.3 The role of automation and control

The focus of most technical literature on submarine geotechnical drills has been on tooling issues. Thus, for instance, Kelleher & Hull (2008) describe a specific piston corer or Nguyen et al. (2013) a SCPTu unit. This emphasis is reasonable because without appropriate tools, geotechnical drills will not recover useful data.

It is also true, however, that speed and relative ease of operation are also likely to be determinant factors in the medium and long-term prospects of remotely operated drills. If operation is too complex or slow their uptake in average surveys will be seriously hindered. Control and automation are two key aspects in this respect but, despite their relevance, there have not been discussed in much detail (a notable exception being the work of Hampton et al., 2016).

This paper aims to partially fill that gap, describing the main elements of the operational control and automation system that have been implemented in a newly developed geotechnical submarine drill, the MD500. These elements are presented after giving a brief overall description of the MD500 project.

Finally, results from several experiments designed to evaluate handling quality and performance of the robotic elements in the machine are also described.

2. General system description

2.1 Specifications

Building on the experience gained in the development and operation of a previous single-shot submarine drill (Romero et al., 2012), Igeotest launched the MD500 project.

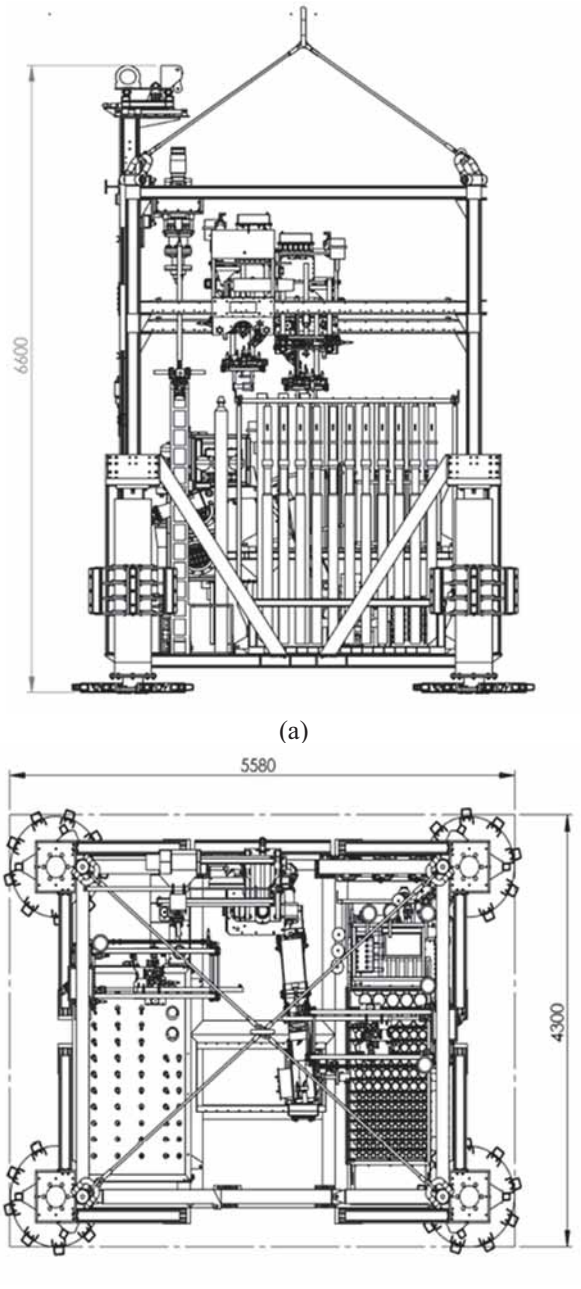

Figure 1: Side and top views of the MD500 machine

General dimensions of the machine assembled for testing are presented in Figure 1.

The main specifications of the MD500 project are:

- Operating depth up to 500m.
- Conventional geotechnical drilling head with mud flow system.

- Drilling diameters: 146mm (GEOBORE S), 84.8mm (PWL), 63.5mm (HWL), 47.6mm (NWL).
- Maximum drilling depth between 88 and 176 m, depending on the initial drilling diameter.
- Tool deployment via either wire-line system or rod assembly.
- Approximate weight on air of 14 kN.
- Modularity. Selecting and assembling of specific tools and/or modules for each survey to perform.

2.2 Modules

The MD500 machine (Figure 2) includes nine main modules: drilling rig (1), anthropomorphic manipulator (2), two Cartesian manipulators (3), stabilizing legs (4), sample tube storage (5), rod storage (6), electric and hydraulic power and communications unit (7), drilling mud system (8) and wire-line sample retrieval tools (9).

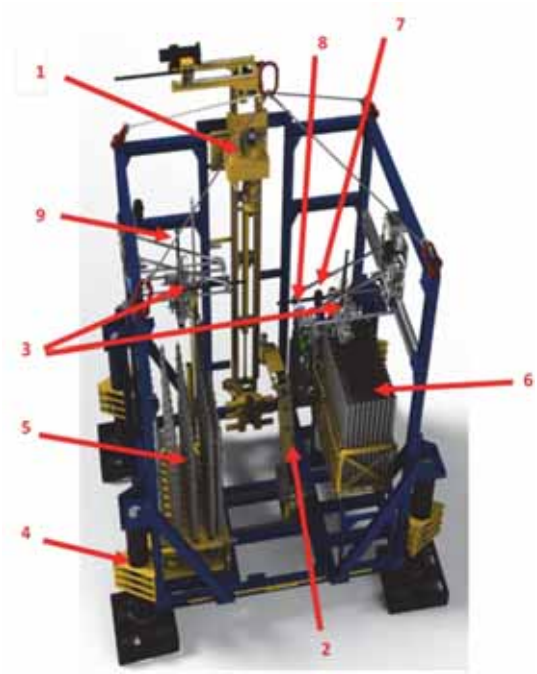

Figure 2: 3D render of the MD500 machine with indication of main components

3. Control and automation

3.1 Distributed control architecture

The main trait of the MD500 control system is a distributed control architecture that relays on six Programmable Logic Controllers (PLC) distributed within the machine. This trait simplifies synchronization and fail-safe procedures, enhancing the operational robustness of the system.

The machine is remotely operated with aid of a Graphical User Interface (GUI) in the master PC. From this application, the operator can select specific semi-automated sequences or send manual commands to be executed by the drilling rig, handling robots or balancing legs. All these instructions are sent via Ethernet to the communications unit, where they are converted into CANbus messages and interpreted by one of the six Bosch Rexroth BODAS RC PLC's installed, respectively, for controlling: the robot arm, Cartesian robots, legs, drilling rig and drilling mud system. Information about the status of the devices is then fed back to the master application and continuously logged into a database.

The different PLC-controlled module operations are effected through several closed loop control algorithms executing in a high-priority program thread. In this way, real time operation of every critical module is ensured, while interfacing and communications with the master PC are managed in a lower priority thread. Further details of the general control architecture of the MD500 can be found in Arriaga et al. (2016a).

3.2 Manipulators

Of particular interest from the point of view of automation and control are the three different manipulators, which were all designed in-house. Two of them are Cartesian robots: in essence, small gantry cranes that handle either the sample tubes or the drilling rods, for storage and to present them to the robot arm at a designated location.

The Anthropomorphic Robot Manipulator or ARM is a 5-DOF (Degree of Freedom) robot arm (Figure 3) which handles the elements fed by the other two robots and places/removes them in/from the drilling rig. Placement/removal from the rig is done while synchronizing with multiple grippers that enable to assemble/disassemble multiple rods and release the sampling tube retrieved by the wire-line system winch. The ARM is designed to handle a payload of up to 300 Kg.

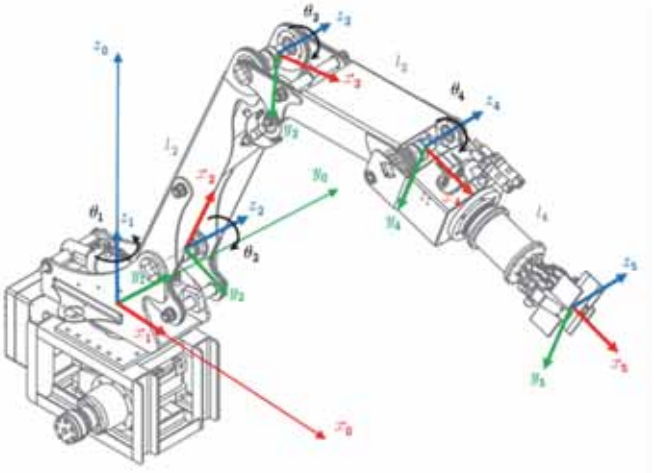

Figure 3: Frame assignment to establish a direct kinematic model of the ARM

3.3 ARM motion control

The ARM is the manipulator tasked with the most varied and difficult tool handling processes. It is therefore the module where robust and precise motion control is more necessary. The MD500 ARM is actuated through a series of hydraulic cylinders and motors, which are regulated mostly through directional proportional electrohydraulic valves.

Ideally, an analytical model is needed in order to accurately control the position of a hydraulic actuator (cylinder or motor) subjected to a known load and operation conditions, making possible to tune the PID controller gains offline and to run simulations in order to guarantee system performance and stability. However, in our particular application the working conditions and number of parameters and variables fluctuate significantly:

- The masses to be handled can vary considerably due to the different kind of soils retrieved, to the unpredictable recovery of any single perforation operation, and to the variety of sizes in sampling tubes and rods to be used. All this makes difficult to estimate "a priori" the effective load.
- The effective applied force, inertia and friction in joints depend upon the angular position of each joint.
- The commanded accelerations and speeds vary according to the operation phase and are adjusted continually.
- The oil variety available may change depending on local conditions. Moreover, for any oil variety essential parameters such as fluid density, viscosity and bulk modulus depend strongly on working temperatures that may vary significantly during a single deployment.

Such varying conditions render analytical operation models unpractical as a basis for model identification procedures. An alternative to address these issues is the use of an adaptive self-tuning fuzzy PID controller, which is able to adjust its parameters using empirically determined rules implemented as a fuzzy inference system.

The Takagi-Sugeno fuzzy approach was therefore implemented in a modified version of the PID algorithm to adjust, in real time, the PID controller parameters of the ARM in its dedicated PLC. The comparative performance of this algorithm and the conventional PID for tracking a sinusoidal reference trajectory while subject to external disturbances is illustrated in Figure 4, where the smoother operation enabled by the fuzzy logic technique is evident. Further details of this aspect may be found in Arriaga et al. (2016b).

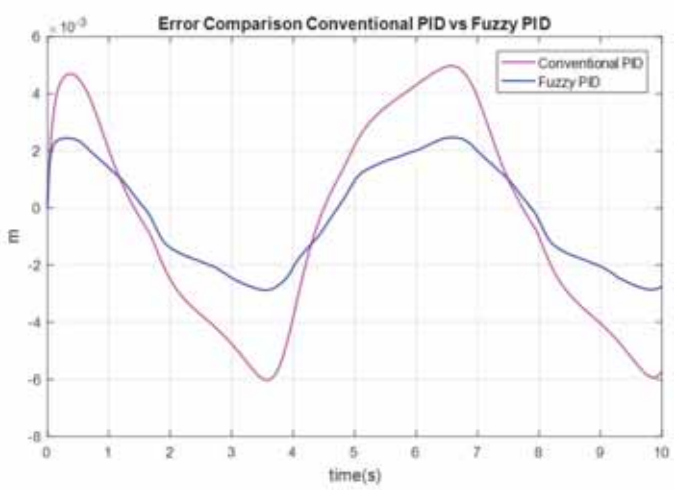

Figure 4: ARM motion tracking error of conventional and fuzzy PID motion control algorithms

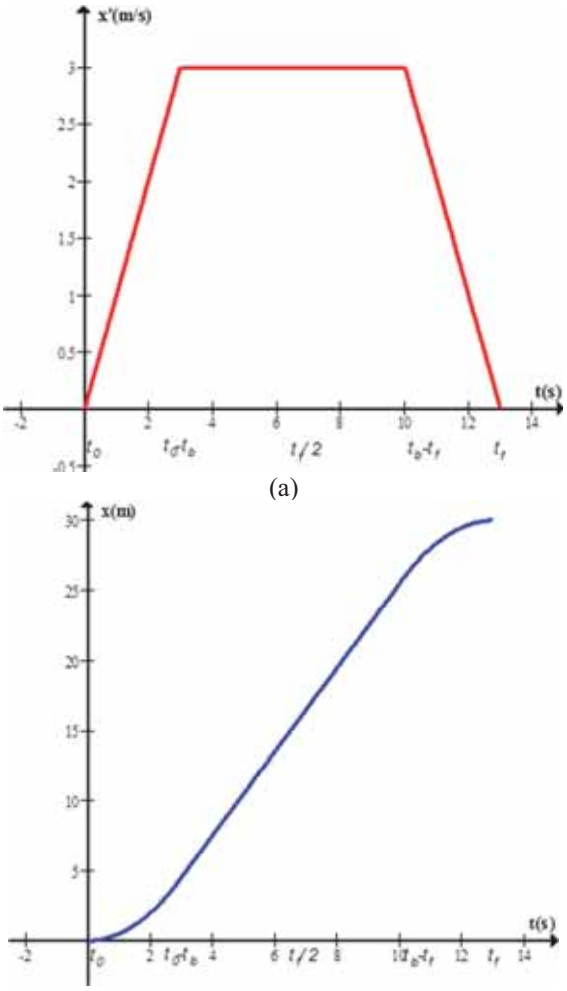

(a)

(b)

Figure 5: (a) Example of velocity ramp and (b) its associated position profile with start/end "blend"

To further smoothen the robot motions, linear acceleration/deceleration ramp motion profiles were implemented through a path generation program that produces in real time the tracking reference for

going from one point to another, i.e. a smooth trajectory is fed to the PID controllers. The purpose is to prevent abrupt motions that may disturb the soil samples. To create a smooth path with continuous position and velocity a linear function is used initially and then a "blend" region is added at the end of each point, as depicted in Figure 5.

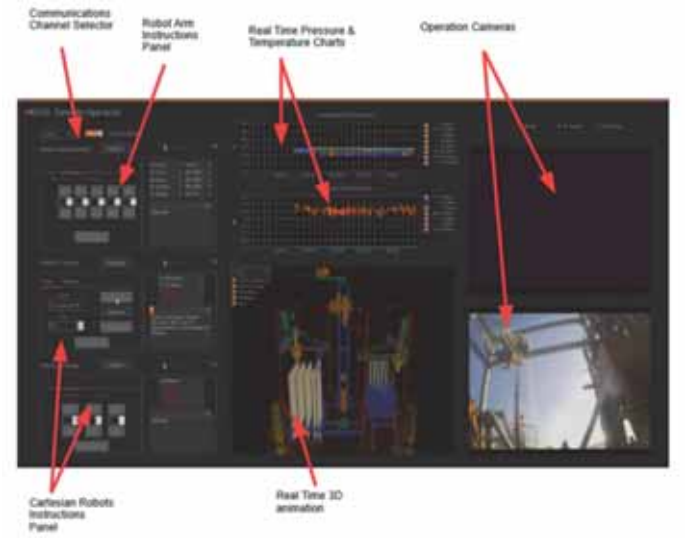

(a)

(b)

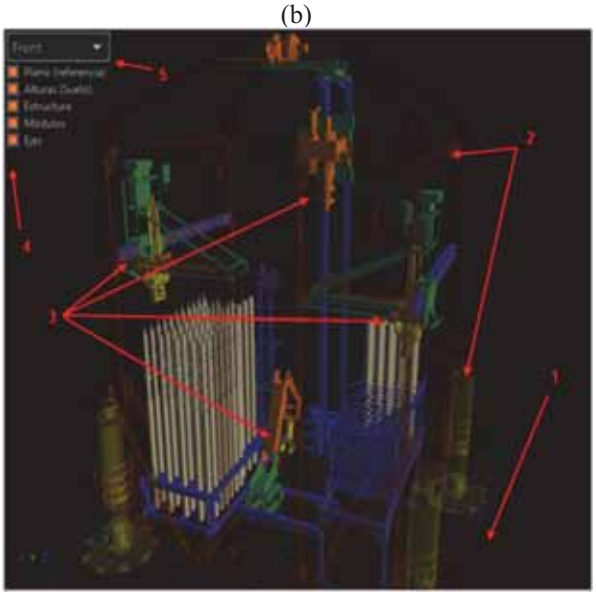

(c)

Figure 6: (a) GUI main screen and (b) GUI in execution in the control post PC (c) 3D real time animation screen

3.4 Graphical User Interface (GUI)

Human remote operation of the MD500 takes place though a graphical user interfaces system, designed to accommodate two operators simultaneously at the command and control centre (Figure 6). Well-developed GUIs can avoid the user from learning complex command languages; thus, a major advantage of GUIs is that they make machine operation (and in our case the operation of the MD500) more intuitive and easier to learn and use.

The actions in a GUI are performed through direct manipulation of graphical elements (e.g. buttons, slide-bars, toggle buttons, drop-down menus), but also with direct user input devices, e.g. keyboard, mouse and joysticks.

The MD500 GUI incorporates a real time 3D animation that represents current machine state (Figure 6c). It was developed using the Microsoft© XNA Framework. This is a source of three-dimensional visual feedback for the operator. In this screen it is possible to enable or disable certain parts of the visualization to render easier the user's tasks and to allow him to focus in precise phases of the equipment deployment and sample retrieval. Although the MD500 includes 12 video cameras for visual feedback, this display was conceived to help the operator under low visibility conditions, which are likely in many operational circumstances.

Figure 7: MD500 prototype assembled at Roses harbour

4. Tool handling experiments

Assembly and initial dry testing of the MD500 took place at Roses harbour in NE Spain (Figure 7), a location selected to facilitate later wet testing, (still ongoing at the time of writing and not reported here). Several special tests were devised to explore the quality and speed of robotic handling operations and to obtain feedback on several aspects of the mechanical design of the machine.

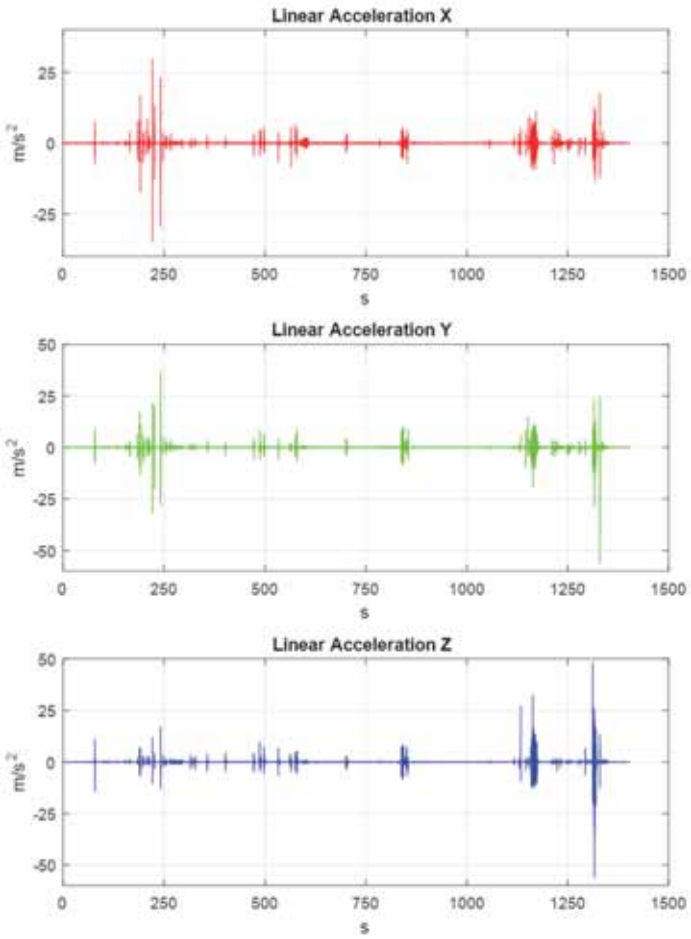

Figure 8: Sampling tube accelerations during one storage operation

4.1 Handling quality

In this kind of test the objective was to obtain an assessment of handling quality by the ARM. To do that, the accelerations suffered by a sampling tube during handling operations had to be registered.

For this purpose an inertial measurement unit (IMU) was attached to the tube. This sensor (Madgwick et al., 2013) allows recording 3-component linear acceleration in autonomous mode (i.e. without cabling), which was ideally suited for the application. Acceleration records obtained for an empty sampling tube during a storage operation performed in semi-automatic operation mode are illustrated in Figure 8.

In the example shown the highest accelerations are noted at the moment (just after the 1250 s mark) in which the gantry robot needed to overcome the force applied by the spring of the locking mechanism in the sampling tubes storage area. This kind of measurement allowed refinement of the detailed mechanical arrangement of sampling tube storage area and default motion speeds for automated handling operations.

4.2 Handling efficiency

In this kind of test the objective was to evaluate the time needed to perform deployment and storage operations of perforation tools using the three handling robots. Three operation modes were evaluated: (i) all robots in manual mode (with closed-loop position control), (ii) gantry robots in semi-automatic mode (predefined routines) and anthropomorphic robot arm in manual mode and (iii) all robots in semi-automatic mode.

The handling tests focused in the one component of the drilling cycle in which robotic handling is more relevant, namely deployment from storage to perforation position of the drilling element and removal of it from perforation position to storage. The results of these tests are summarized in Table 1, where the superior performance of the fully semi-automated mode of operation is evident.

Table 1: Time (in minutes) for tool handling at initial trials

Operation Mode	Deployment	Storage
Manual Gantry & Manual Robot Arm	55’	50’
Semi-automatic Gantry & Manual Robot Arm	34’	28’
Semi-automatic Gantry & Semi- automatic Robot Arm	24’	20’

An additional benefit of these tests is that they revealed how small adjustments of the morphology of gripping end effectors in the robots could significantly reduce the handling operation times. The attainable time reduction upon modification of the mechanisms could be precisely evaluated by analysing the time record of the operations and is presented in Table 2.

4.3 Drilling and sampling sequence

Drilling took place on the dock location of the MD500 and therefore the material being perforated was the granite rockfill mound that sustains the dock. Double barrel rotary drilling using a PWL (84.8 mm) drill bit with diamond inserts was the appropriate technique for sampling this -rather hard- material. Drilling advance took place at a linear feed

rate of 1 cm/min and a rotational speed of 800 RPM and 80 bar of pressure.

The information from drilling and handling tests may be combined to evaluate, under different hypothesis, full cycle sequences of drilling and sampling for an advance of 1.5m. For instance, using the improved end-effectors and drilling rockfill, the cycle time needed to deploy a 1.5m sampling tube, drill, retrieve and store the tube would be roughly 32 minutes. Details of the tasks of this cycle are presented in the Gantt chart illustrated in Figure 9.

Table 2: Effect of end effectors morphology

Task	Attainable Time Reduction
Sampling Tube Deployment Phase 1 (Gantry)	20.0%
Sampling Tube Storage Phase 1 (ARM)	46.2%
Sampling Tube Storage Phase 2 (Gantry)	22.2%
Sampling Tube Deployment Phase 2 (ARM)	70.0%

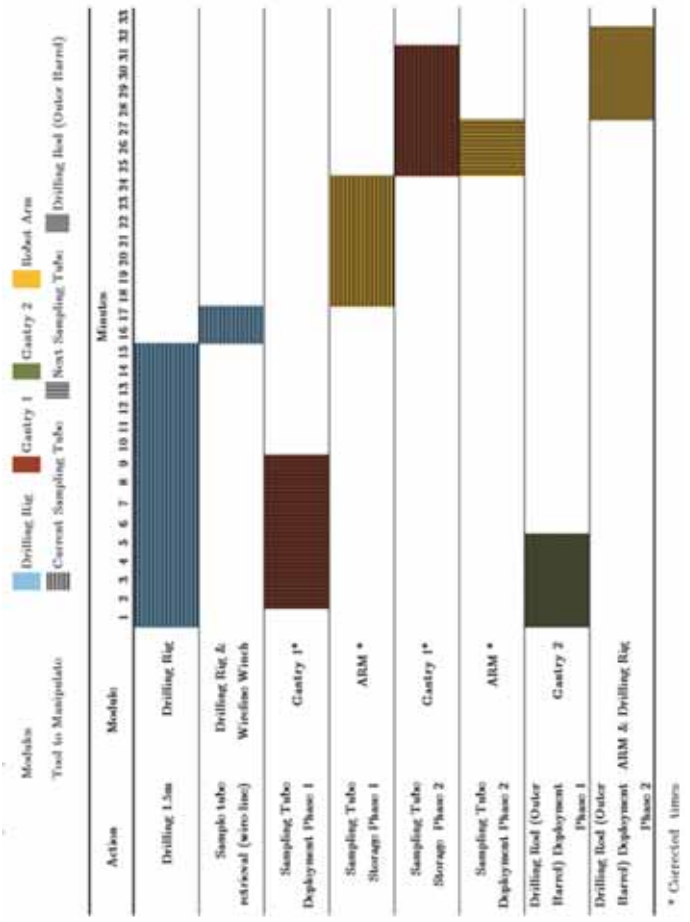

Figure 9: Gantt chart of sampling and storage procedure for a 1.5 m rock drilling and sampling advance (enhanced end effectors)

There are few reports of operational performance of underwater drilling rigs that may be used as reference for comparison with these cycle times. An exception is the work by Yetginer & Tjelta (2010), who contrast drilling and sampling from vessel and a seabed drilling machine.

Their results show that for a 40m sampling depth at 1300 m of water depth, a drilling vessel would take an average of 3.3 days (maximum 5.8 days) while the seabed drilling approach would take in average 0.5 days (maximum 0.6 days). According to the cycle time per 1.5m of sample (32 minutes) and the Gantt chart presented in Figure 9, the time needed for the MD500 to obtain 40 m of soil sample would be 14.4 hours (0.6 days), which lies within the range given by Yetginer & Tjelta (2010) for sampling a 40 m continuous borehole. It should be noted also that the database compiled by Yetginer & Tjelta (2010) referred to a very different material (soft soils). It is likely that the drill/sampler advance times of the MD500 in such material would be significantly smaller than those due to rock drilling reported in Figure 9.

5. Conclusions

A basic challenge for a remotely operated submersible drilling rig is to ensure robustness in communications with the virtual drilling crew operating it from the surface. The MD500 aims to tackle this challenge through the implementation of decentralized control architecture for coordinating the tasks of handling robots and drilling rig. This makes possible to give a relative grade of independence to the handling robots through the utilization of predefined semi-automatic routines, allowing the operators to centre their attention in drilling tasks. Closed loop control in handling robots axes and joints enable the system to guarantee repeatability and motion/position accuracy in such automated tasks.

A second important consideration is to ease the interaction between operator and machine. The GUI incorporated in the control post PC provides the interaction channel between the operators and the machine. It aims to further help the driller tasks by providing relevant data of the machine state in real time, including visual feedback (cameras) and real time 3D animations envisioned to yield guidance in very likely low visibility conditions. It was designed to be intuitive and easy to use, eliminating the need of learning complex commands for the machine operation, thus reducing the learning curve for new users.

Initial operation tests suggest that the system can perform drilling, sampling and associated tasks at a pace fast enough to be comparable to other pieces of

equipment commercially available. Further tests are planned to refine the MD500 control routines and mechanical design and to optimize the cycle time per operation.

Handling quality experiments have been devised to measure the quality of robotic manipulation. It is planned to repeat these experiments during future testing campaigns and relate them to direct measurements of sample quality. This approach, it is hoped, will further clarify the link between automation and quality of sampling, which is the desired end product from such equipment.

6. Acknowledgement

The authors acknowledge the support received from the Spanish CDTI through projects IDI-20130847 and SERA20151003. The first author work was supported through an Industrial Doctorate grant by the Catalan Autonomous Government.

7. References

Arriaga A, Arroyo M and Pérez N. (2016a). The Virtual Drilling Crew. In Proceedings of 1st IMEKO TC4 International Workshop on Metrology for Geotechnics, MetroGeotechnics 2016 (pp. 318-321).

Arriaga AG, Arroyo M, Pérez N and Devincenzi M. (2016b) Control Strategies for an Underwater Geotechnical Drilling System. EACS 2016, 6th European Conference on Structural Control, Paper 180

Carter JP, Davies PJ and Krasnostein P. (1999). The future of offshore site investigation–robotic drilling on the sea-bed. Australian Geomechanics, 34(3), 77-84.

Hampton PJ, Soylu S, Crees T and Jackson E. (2016, May). Improvements and Capabilities of the CRD100 Subsea Robotic Drilling Platform. In Offshore Technology Conference. Offshore Technology Conference.

ISO 19901-8, "Petroleum and natural gas industries - Specific requirements for offshore structures", Part 8: Marine soil investigations, 2014.

Madgwick SO, Harrison AJ, Sharkey PM, Vaidyanathan R and Harwin WS. (2013). Measuring motion with kinematically redundant accelerometer arrays: Theory, simulation and implementation. Mechatronics, 23(5), 518-529.

Nguyen HQ, Kelleher P, Degroot D, Lunne T, Senders M and Banimahd M. (2013, May). Offshore site characterization of small strain shear modulus using a seabed based drilling system. Offshore Technology Conference. OTC-24124-MS.

Pennington D and Kelleher P. (2007, January). PROD delivers an accurate site investigation at Maari. In Proceedings 6th Offshore Site Investigation and Geotechnics Conference. Society of Underwater Technology.

Romero F, Devincenzi MJ, García NP, Arroyo M and Deu A. (2012). Testing a New Submersible Drill Rig. 7th Offshore Site Investigation and Geotechnics Conference. Society of Underwater Technology.

Spencer AG, Remmes B and Rowson I. (2011, January). A fully integrated solution for the geotechnical drilling and sampling of seafloor massive sulfide deposits. Offshore Technology Conference. OTC-21439.

Spagnoli G and Freudenthal T. (2013). Underwater drilling rig for offshore geotechnical explorations for Oil & Gas structures. Oil gas European Magazine, December.

Spagnoli G, Finkenzeller S, Freudenthal T, Hoekstra T, Woollard M, Storteboom O and Weixler L. (2015, September). First Deployment of the Underwater Drill Rig MeBo200 in the North Sea and its Applications for the Geotechnical Exploration. In SPE Offshore Europe Conference and Exhibition. SPE-175456-MS

Tirey GB. (1972). Recent trends in underwater soil sampling methods. Underwater Soil Sampling, Testing, and Construction Control, ASTM STP, 501, 42-54.

Yetginer AG and Tjelta TI. (2010). Seabed drilling vs surface drilling–a comparison. Proceedings of Frontiers in Offshore Geotechnics II. ISFOG, Perth. Gourvenec and White, Taylor & Francis Group, 327-331.

COMMON PITFALLS OF PILE DRIVING RESISTANCE ANALYSIS – A CASE STUDY OF THE WIKINGER OFFSHORE WINDFARM

RM Buckley, S Kontoe, RJ Jardine
Imperial College London, London, UK

M Maron
Fugro Geoconsulting SAS, Paris, France

FC Schroeder
Geotechnical Consulting Group LLP, London, UK

P Barbosa
Iberdrola Renewables Offshore Deutschland, Berlin, Germany

Abstract
Pile driving resistance analyses are often performed to provide indicative information on potential axial static capacity. This involves a well-established approach, commonly known as signal matching, in which dynamic measurements made during impact driving are related to estimates of shaft and base resistance through wave propagation theory. The dynamic traces can theoretically be matched by more than one distribution of shaft and base resistance. As the solution process is not unique, the estimated capacity is inherently more subjective and less reliable than capacities obtained from static testing. The effects of time (set-up) and loading style must also be considered. This paper focuses on the sensitivity of signal matching predictions considering the effect of various shaft and base soil resistance models, as well as more practical aspects concerning the operator and software dependency of the predictions. The response, at the end of driving and at the beginning of restrike, of two hollow steel piles driven in two distinct ground profiles is analysed with three software codes (CAPWAP, Allwave-DLT & IMPACT), considering simple and more advanced soil resistance models. The results highlight the uncertainty in signal matching simulations, and the requirement for confirmation with static testing.

1. Background

Dynamic pile testing (DPT) is used routinely as a relatively economical means of gaining indicative information on static pile capacity. During a hammer blow, recordings from strain gauges and accelerometers near the pile head allow time histories of pile force and velocity to be determined. Pile capacity can then be obtained by idealising the response as a one dimensional (1D) wave propagation problem (Isaacs, 1931). However, it is well accepted that static testing is essential to the verification of dynamic pile tests (Svinkin, 2004).

Iberdrola are employing DPT for the Wikinger offshore wind farm in the Baltic Sea (Barbosa et al., 2015), which includes 70 (No.) 5MW wind turbine generators (WTG) and an offshore substation. A first, pre-construction pile testing programme was completed in early 2015 at the site, with novel axial static and cyclic pile tests on the sea bed, in water depths up to 42m, on 1.37m diameter (D) open ended steel tubes. The test piles penetrated up to 31m of Weichsellian glacial deposits and Maastrichtian chalk.

As part of this programme, dynamic tests were conducted on 3 piles at the same time as adjacent static tests, up to 108 days following end of driving (EoD). The later production piling was completed in 2016 with 286 (No.) 2.7 to 3.76m diameter piles. Dynamic tests were carried out on 14 piles during driving; instrumented restrikes were completed on nine piles up to 67 days after EoD.

A Joint Industry Project (JIP) is currently underway between Iberdrola, Imperial College London and the Geotechnical Consulting Group which aims to improve design reliability in chalk. Onshore field testing programmes on driven and jacked piles which also form part of the JIP were described by Buckley *et al.* (2017a, 2017b). Analysis of DPT data at Wikinger forms part of the JIP and this paper presents the approach taken with a particular focus on:

1. Numerical methods and soil resistance models to assess DPT in chalk and glacial till;
2. Available analysis software;
3. Potential operator dependency of the signal matching solution, and;
4. Comparison of DPT results with corresponding static load tests.

2. Numerical Methods

Analysis of force (F) and velocity times pile impedance (ZV) signals obtained from a hammer blow is known as signal matching. Signal matching analysis is usually performed using dedicated programs, such as CAPWAP, Allwave-DLT or IMPACT, which are based on one of two numerical methods to model the 1D wave propagation problem: Smith's (1962) lumped mass finite difference approach or the Method of Characteristics (MOC) (De Josselin De Jong, 1956). For both methods, the measured ZV signal is generally used as the input boundary condition and the aim of the analysis is to match an artificially generated signal for the returning upward force with the measured one. For a free beam, the artificial signal differs from the measured one by an amount equal to the total soil resistance. Therefore, the signal matching approach consists of iteratively changing soil resistance along the pile, by varying input parameters to the adopted soil resistance model, until a good quality match is obtained. The parameters obtained in this way should not be considered as a unique set, but rather as a best fit to the particular data set, as obtained by one user.

3. Soil resistance models

3.1 Traditional models

Traditional models used to represent base resistance and shaft resistance for each node along the pile are derived from the rheological models of Smith (1962). The models, illustrated in Figure 1, consist of a linear spring and plastic slider in parallel with a viscous dashpot, which represents all soil damping effects. The spring represents the relative movement of the pile and soil prior to the limit of the plastic slider. Total soil resistance (R_t) at each node is therefore the sum of the static resistance (R_s) and the dynamic resistance (R_d):

$$R_t = R_s + R_d = Kw + Cv \qquad \text{Eq. 1}$$

Where K and C are the spring and dashpot constants, respectively, v is the velocity of the pile and w is the pile displacement. A shaft damping parameter, J_s with units of s/m, was introduced by Smith to simplify the problem in terms of computational effort, such that Eq.1 becomes:

$$R_t = R_s(1 + J_s v) \qquad \text{Eq. 2}$$

The shear stress, τ along the pile shaft can then be written as:

$$\tau = \min(k_s w, \tau_s)\,(1 + c_s v) \qquad \text{Eq. 3}$$

$$k_s = \frac{K_s}{A_s} = \frac{\tau_s}{U_{q,s}} \qquad \text{Eq. 4}$$

$$c_s = \frac{C_s}{A_s} = J_s \tau_s \qquad \text{Eq. 5}$$

Where, A_s is the shaft area and $U_{q,s}$ is the shaft soil "quake" or displacement required to fully mobilise the static shaft resistance, τ_s. Base resistance is represented in a similar manner to Eqs. 1 to 5.

The limiting shaft and base resistances are assessed based on the soil conditions. Values of quake (U_q) and damping (J), obtained from back analysis of driving records and comparison with static tests, normally lie within a relatively narrow range. U_q is generally between 2 and 5mm and a value of 2.54mm (1 inch) is often adopted. Similarly, shaft damping (J_s) usually falls between 0.1 and 0.6s/m and base damping, (J_b) is often assumed to be around 0.5s/m (Hannigan *et al.*, 2006).

Several Authors have proposed modifications to the Smith damping constants (J_s and J_b) based on laboratory testing that shows a non-linear relationship between soil strength and velocity (Coyle and Gibson, 1970, Dayal and Allen, 1975, Litkouthi and Poskitt, 1980). A power law relationship in place of Eq. 2 may be adopted:

$$R_t = R_s(1 + \alpha v^{\beta}) \qquad \text{Eq. 6}$$

Where α and β are viscosity parameters. Randolph (2008) recommends β = 0.2, and α between 0 for a dry sand and 1 or higher for clay soils. Asymmetric elasto-plastic springs have also been suggested in place of traditional linear springs. These use so called "Yield Factors" to model lower tensile shaft resistance on unloading than on loading and allow better matching of the force signal.

In "coupled" analyses, the dynamic resistance is a function of the static resistance (τ_s) as in Eq. 3 to 5. For uncoupled analyses, the spring, dashpot and slider have the same configuration, but the parameters relating to static and dynamic resistances (k_s and c_s) are defined independently of τ_s. A typical Smith model coupled response at a pile shaft node is shown on Figure 2 using the EoD blow for one of the Wikinger test piles.

It should be noted that the dynamic part of this form of the soil resistance model does not explicitly consider the inertia of the surrounding soil, the effects of radiation damping in the far-field nor does it differentiate between behaviour before and after pile slip. The internal shaft resistance is also not considered separately to the external resistance.

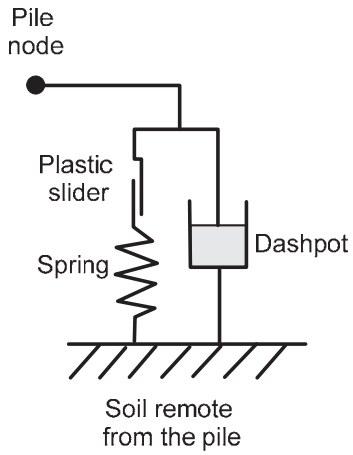

Figure 1. Traditional soil resistance models (after Smith, 1962)

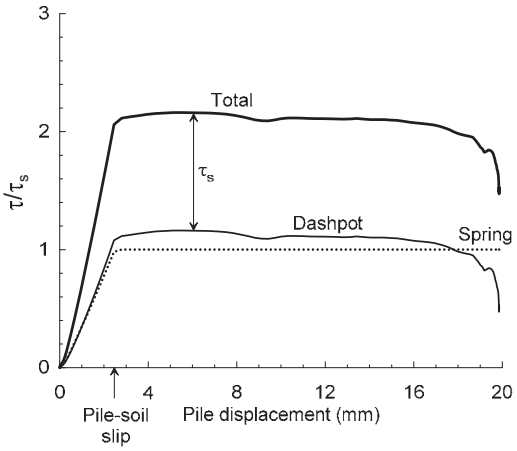

Figure 2. Typical Smith model response for a pile shaft node

3.2 Rational models

Several other rheological models have been proposed to better simulate the mechanics of pile driving (e.g. Randolph and Simons, 1986, Holeyman, 1985, Deeks and Randolph, 1995, Salgado et al., 2015). In the present study, two models have been considered, whose parameters are linked to measurable soil properties.

The Randolph and Simons (1986) shaft model, shown schematically on Figure 3, is based on the analytical solution of Novak et al. (1978), and accounts for both viscous damping at the pile-soil interface and radiation damping in the far-field. Radiation damping is more important when nearly elastic displacement occurs such as when piles are driven close to refusal, while viscous effects are dominant where primarily plastic sliding is occurring (Danziger *et al.*, 1999). In the Rational model, at each pile node, the shear stress, τ is given by:

$$\tau = G\left(\frac{w_s}{D} + \frac{v_s}{V_s}\right) \qquad \text{Eq. 7}$$

Where w_s and v_s are the soil displacement and velocity, G is the shear modulus and V_s is shear wave velocity ($\sqrt{G/\rho_s}$) where ρ_s is the soil density. The shear stress at the interface,$\tau_{inter,}$, is calculated as a function of the relative slip velocity between pile and soil Δv, the static resistance $\tau_{s,}$, and a normalising velocity v_0 (=1m/s):

$$\tau_{inter} = \tau_s\left(1 + \alpha\left(\frac{\Delta v}{v_0}\right)^{\beta}\right) \qquad \text{Eq. 8}$$

Values for the viscosity parameters α and β are given previously. The internal soil column is modelled independently in a similar manner to Eq. 7 and Eq. 8.

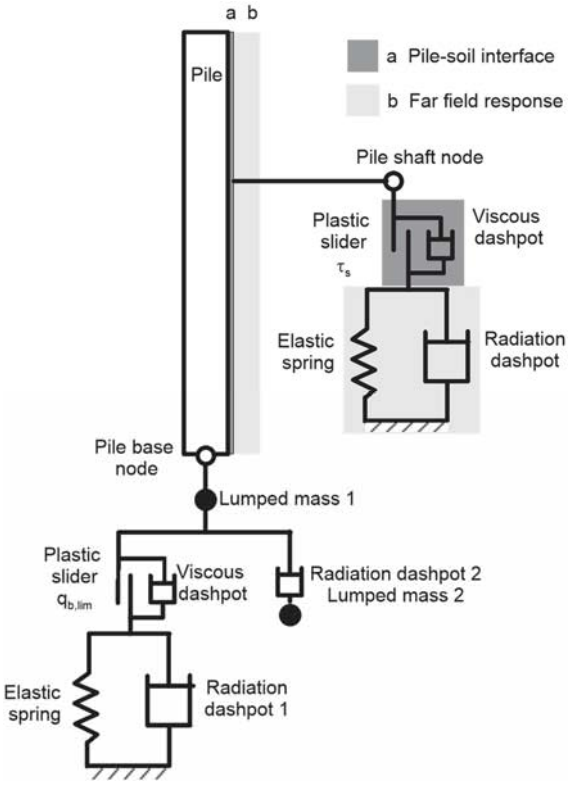

Figure 3. Rational soil resistance models (adapted from Randolph and Simons, 1986, Deeks and Randolph, 1995)

Figure *4* shows a typical response for the same pile shaft node and hammer blow as for the traditional model in Figure 2. Radiation damping can be seen to dominate the response initially. Pile-soil slip occurs at very small displacements (≈0.1mm), when the total (spring plus radiation dashpot) shear stress reaches the limit of the plastic slider τ_s. The spring and dashpot are then disconnected and the soil and pile displacements are calculated separately. The behaviour during slip is only controlled by the slider and the viscous dashpot. Nonetheless, the spring and radiation dashpot components continue to be calculated, as shown in Figure *4*, and when the shear stress (calculated using the pile velocity and soil displacement) reduces below τ_s the spring and radiation dashpot are re-engaged.

The response shown in Figure *4* can be directly compared to the Smith model response (Figure *2*) where the modelled initial response is significantly softer. Similar peak strengths are mobilised between the two models although peak resistance is reached more gradually with the Smith model.

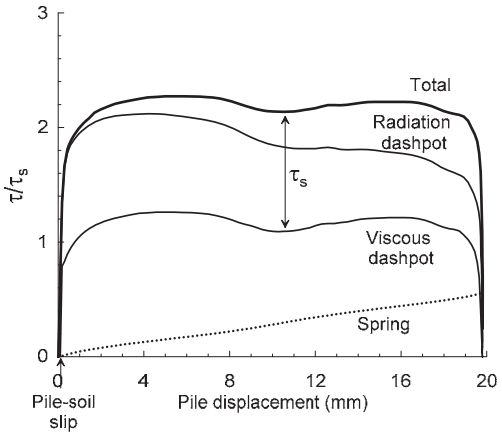

Figure 4. Typical rational model response

The Deeks and Randolph (1995) base model, also shown in Figure 3, is similar to the shaft model described above, but also includes lumped masses connected through the base (m_1) and a second radiation dashpot (m_2). The base spring stiffness can be calculated from:

$$k_t = \frac{2GD}{1-\nu} \qquad \text{Eq. 9}$$

Where ν is Poisson's ratio; for undrained conditions, $\nu = 0.5$ and $m_2 = 0$. The radiation dashpot in parallel with the elastic spring, c_b and m_1 are defined as:

$$c_b = \frac{0.85D^2}{1-\nu}\sqrt{G\rho_s} \qquad \text{Eq. 10}$$

$$m_1 = 0.16D^3\rho_s \qquad \text{Eq. 11}$$

4. Unknowns in signal matching

An indicative list of unknowns when undertaking wave equation analyses in typical commercial codes (e.g. CAPWAP and Allwave) is given in Table 1. There are $3N_s + 3$ primary unknowns, where N_s is the number of pile shaft nodes. The remaining parameters are only used to improve match quality and do not affect the mobilised resistance. This increases the number of unknowns to $3N_s + N_p + 8$, where N_p is the number of elements in the internal soil plug. The choice of dynamic parameters has a significant effect on driveability predictions, particularly in conditions where typical parameters are not available.

The Rational soil models have been implemented in IMPACT (Randolph, 2008). The unknowns in this case are shown in Table 3. The addition of the non-linear dependence of strength on velocity increases the primary unknowns to $5N_s + 3$. Although there remains uncertainty in the selection of the viscosity parameters, typical values of α and β have been given previously. Applying these reduces the number of unknowns to $3N_s + 3$, i.e. the same as the number of primary unknowns in typical commercial codes.

The displacement generated by a hammer blow during DPT is generally significantly less than the limit of 10% of the pile diameter commonly used to define static failure. Therefore full base capacity is rarely mobilised during DPT. As a result, pile driving prediction methods often include a factor to account for this partial mobilisation which increases the number of unknowns for both the traditional and rational models by 1; e.g. Byrne et al. (2012).

Table 1. Summary of unknowns in typical commercial codes

Parameter	*No.*	*Type*
Shaft resistance	N_s	Primary unknown
Base resistance	1	Primary unknown
Shaft quake	N_s	Primary unknown
Base quake	1	Primary unknown
Shaft damping	N_s	Primary unknown
Base damping	1	Primary unknown
Shaft unloading quake	1	Improve match
Base unloading quake	1	Improve match
Yield factor	1	Improve match
Base gap	1	Improve match
Base plug	1	Improve match
Shaft plug	N_p	Improve match

Table 2. Summary of unknowns using IMPACT

Parameter	*No.*	*Basis*
Shaft resistance	N_s	In situ tests
Base resistance	1	In situ tests
Shaft spring stiffness	N_s	G
Base spring stiffness	1	G
Shaft radiation dashpot	N_s	G,ρ_s
Base radiation dashpot	1	G,ρ_s
Viscosity parameters	$2N_s$	Empirical

5. Comparison between numerical methods

The most widely used signal matching code in industry is the Case Pile Wave Analysis Programme (CAPWAP) which uses Smith's lumped mass finite difference approach and traditional soil resistance models (Rausche et al., 1985). Allwave-DLT also utilises traditional soil resistance models, but the alternative MOC approach as discussed by Middendorp and Verbeek (2006). A direct comparison of these two codes was made for the JIP to assess whether the implementation of the traditional soil resistance models together with the different numerical methods adopted in the two codes leads to similar results.

From the Wikinger site dataset, an EoD blow from one of the dynamic restrike tests was selected for comparison. Cone penetration tests (CPT) were available at all of the sites considered with typical profiles of cone resistance, q_c, sleeve friction, f_s and pore pressure, u_2 given in Figure 5. The ground conditions generally consist of glacial deposits of stiff clay and medium dense sand underlain by Grade A1/B2 low to medium density structured chalk. In some cases, structureless (Grade Dc/Dm) chalk is found immediately below the glacial deposits.

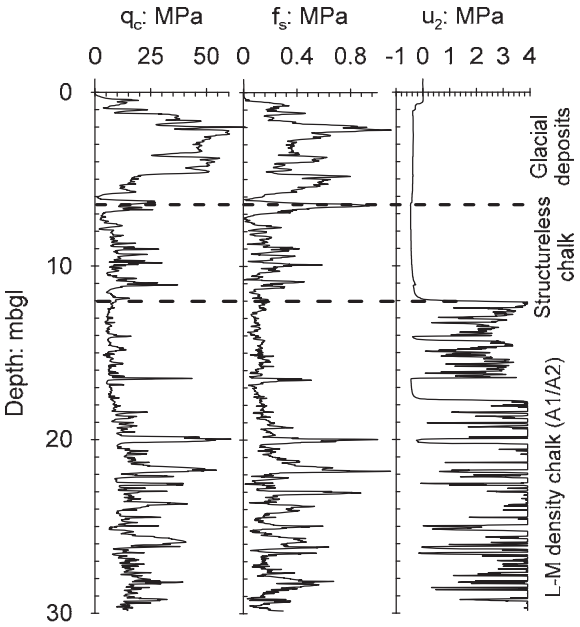

Figure 5. Example profile at the Wikinger test sites

Signal matches were performed by the same operator with CAPWAP and Allwave-DLT using the same model parameters. By default, CAPWAP uses a Smith coupled approach to calculate damping forces (Eq. 5). In Allwave-DLT an uncoupled analysis was performed via the so-called TNO soil model, where the damping factors can be input separately from the static capacity. The first estimates of shaft and base resistances input in CAPWAP were gauged from the available borehole logs, CPTs and down-hole seismic logging. The mobilised shaft resistance and stiffness calculated from the CAPWAP analysis were then input into Allwave-DLT. The dashpot coefficients were calculated from J_s, assumed in the CAPWAP analysis from Eq. 5. The key parameters for both codes are summarised in Table 1.

The calculated upward travelling force waves obtained from both programs are compared with the measured signal on Figure 6. The predictions can be seen to closely match the measured signal and be almost identical between the codes; small differences are observed in the latter portion of the record which can be attributed to differences in the interpolation of the parameters between shaft nodes. For the calculated overall static shaft resistances both codes indicate 32MN with 1MN mobilised at the base.

Table 3. Summary of parameters used in software comparison

Parameter	*Value*
Shaft damping, J_s	0.65
Base damping, J_b	1.38
Shaft quake, $U_{q,s}$ (mm)	3.5
Base quake, $U_{q,b}$ (mm)	2.3
Yield factor (%Q_{tot})	25
Unloading shaft quake (%$U_{q,s}$)	100
Unloading base quake (%$U_{q,b}$)	30

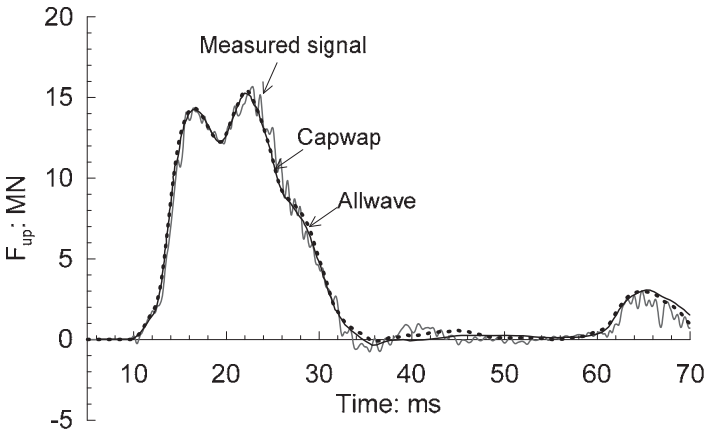

Figure 6. Comparison of upward travelling waves

6. Operator dependency

Uncertainty in the interpretation of DPT has been discussed by several authors (e.g. Danziger et al., 1996, Svinkin, 2004, Chambers and Lehane, 2011). Fellenius (1988) describes a study where 19 participants each performed CAPWAP analyses of four blows, of varying complexity. This resulted in variations from the mean total capacity of between 5 and 14%. The variation in base resistance is not discussed in detail although it is reported as the primary reason for the deviations.

To investigate the effect of different operators on the analysis of the Wikinger data set, the restrike blow discussed above was analysed by three independent operators, using CAPWAP. Only the site investigation data, measured signal and pile dimensions were shared. The choice of soil resistance model and associated parameters was made by the individual analysts. As well as varying the standard Smith parameters Operator 3 used the optional extension of shaft radiation damping, to consider the far-field damping response in conditions of hard driving.

The resulting mobilised shaft resistance obtained from all three signal matches is shown in Figure 7. The interpretations made by the three operators were qualitatively similar, e.g. a lower resistance band was interpreted between 18 and 22m depth which was unexpected from the given site profile. The CAPWAP match quality, MQ (Rausche *et al.*, 2000) obtained by all three operators was between 1.7 and 1.9, indicative of a good quality match.

The total shaft capacity (R_s) estimates fell within ±4% of the mean. Significant differences in the split between base (R_b) and shaft resistance (R_s) were obtained, highlighting the non-uniqueness of the solution, particularly at the base. The differences in base capacity predictions led to total capacities (R_t) falling within approximately ±10% of the mean value. It is worth noting that very similar shaft and overall capacities were obtained by operators 1 and 2, who used the same soil resistance model.

Signal matching is inherently more difficult in situations where the overall resistance is low (easy driving conditions) due to lower shaft resistances and less clear reflections in the time up to t_m+2L/c, where t_m is the time corresponding to the maximum force in the downward travelling wave, L is the pile length and c is the wave speed. To assess operator dependency for such conditions, analyses were carried out by two operators, for an EoD blow for one of the Wikinger piles where the total resistance was low. The mobilised shaft resistance profiles indicated in Figure *8* show a different qualitative interpretation between the two operators. The operators could only obtain MQ values between 4 and 5, indicative of a lower-quality match. Despite the variation in interpreted distribution of shaft friction, the variation in total shaft capacity was within ±4% of the mean value. The overall capacity was within ±2% of the mean value.

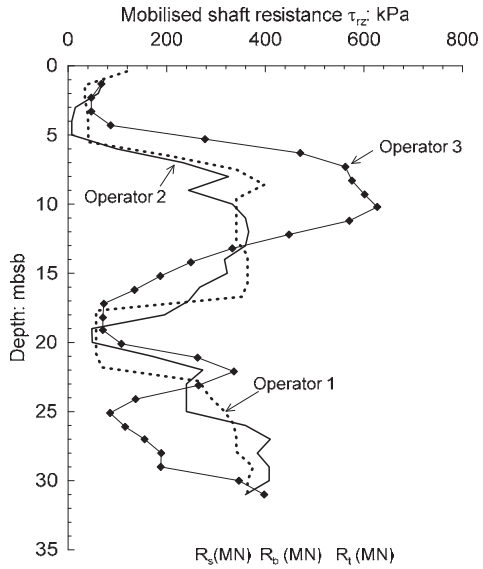

Figure 7. Example operator dependency

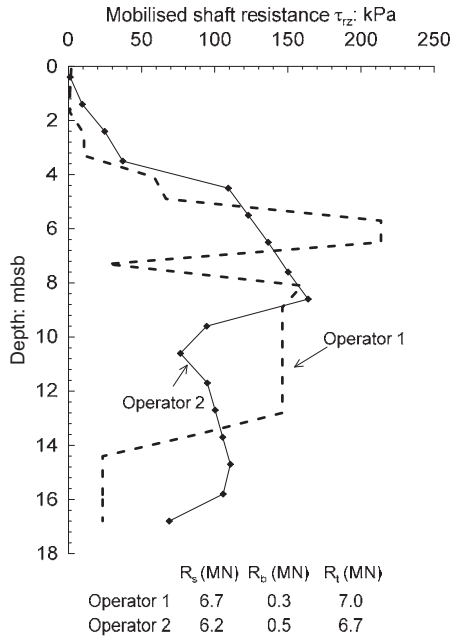

Figure 8 Example operator dependency

7. Comparison with static load tests

The testing carried out at Wikinger allows comparison between the compressive shaft resistance mobilised by the dynamic restrike tests and the tension shaft resistance mobilised during the corresponding static load tests. Using, IMPACT, both the traditional Smith and Rational soil models have been used to analyse blows at EoD and Beginning of Restrike (BoR) for a given pile, at a site where the ground conditions primarily consisted on glacial deposits.

The parameters used in the Smith traditional model are similar to those shown in Table 1. For the Rational model the values of G used were equivalent to ≈20% G_{max}, with G_{max} determined from the results of P-S logging at the site. Salgado *et al.* (2015) showed that the Rational models performed better when G was taken as a degraded secant modulus to reflect soil non-linearity, rather than G_{max}. The initial soil profile was assessed from soil investigation data.

IMPACT includes explicit modelling of the internal shaft resistance for the Rational soil resistance models described in Eq. 7 and 8. For the fully coring piles considered here, the best quality matches were obtained with either low ratios of R_{int}/R_{ext} (<10%) or R_{int}/R_{ext} =0, where R_{ext} and R_{int} are the external and internal shaft capacity respectively. To simplify the analyses, it was assumed that all shaft capacity acts on the external shaft area. A similar conclusion for sands from instrumented field tests was reported by Brucy et al. (1991) and Jardine et al. (2005).

The mobilised shaft resistance profile obtained with the Smith and Rational model are shown on Figure *9*, while Figure *10* compares the calculated upward travelling force waves for the restrike blow with the measured signal. The primary difference between the two models relates to the distribution of mobilised shaft resistance in the lowermost elements and the mobilisation of base resistance. At both EoD and BoR the Rational model indicates a strong dependency of shaft resistance on distance from the pile tip, with significant increases in shaft capacity near the tip. However, the overall shaft resistances (R_s) were within 0.3MN of each other for both hammer blows. The base resistance required to achieve a good match was 3 to 6 times higher with the Rational model than with the Smith model and equated to ≈0.8q_c assuming end bearing acts on the annular pile base area only.

Comparison of the EoD and BoR shaft resistances (Figure *9*) indicates an approximate doubling of resistance over this period. Time effects on base capacity are more difficult to define due to the dependence of capacity on mobilised pile tip displacement.

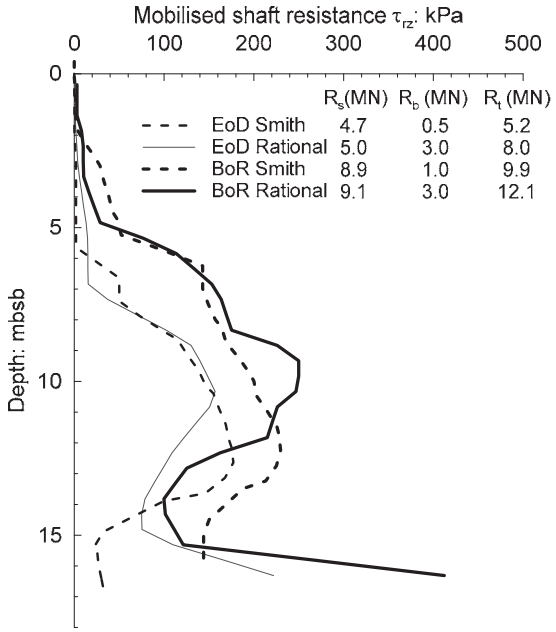

Figure 9. Shaft resistance mobilised by Smith & Rational models

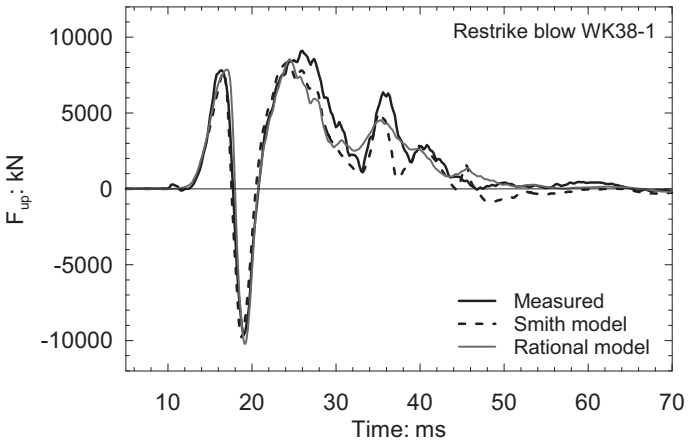

Figure 10. Comparison of upward force wave using two models

The corresponding test pile had a net static failure load, excluding the pile and soil self weight, $R_{s,net}$ of 8.8MN, 108 days after EoD. Reverse end bearing is not considered to have occurred for these piles founded in essentially free draining structured chalk. Therefore, $R_{s,net}$ can be compared with the shaft resistance, $R_{s,dyn}$, from the BoR signal match carried out at the same pile age, assuming that the tensile shaft friction from the static test equates to the compressive shaft friction from the dynamic test.

Capacity obtained from a static tension test is dominated by external shaft resistance. Therefore, the interpreted split between internal and external shaft resistance using the traditional soil model is critical when comparing static and dynamic tests. The capacities, shown in Figure 9, indicate a good correlation between the static and dynamic tests with $R_{s,net}/R_{s,dyn} \approx 1$ either where the internal shaft resistance has been considered separately in IMPACT or assuming that all of the friction mobilised using the traditional models acts on the outside of the pile. In contrast, the assumption that 50% of total shaft friction acts on the inner shaft area, which is common practice in DPT analysis and in pile driving predictions, results in $R_{s,net}/R_{s,dyn} \approx 2$. The latter highlights the significance of this assumption when correlating static and dynamic tests and the requirement for static load tests on similar piles at the same site to verify dynamic analyses.

8. Conclusions

A number of analyses have been presented in which the merits of various signal matching techniques have been explored. The primary conclusions are:

- The traditional soil models used widely in DPT analysis have some limitations, including difficulties linking their input parameters to measurable soil quantities. Nonetheless, for the cases considered they resulted in similar shaft capacities with the primary difference being in the estimation of base capacity;
- For the examples considered, there is no significant difference between the response of the particular traditional resistance model implemented with two numerical methods; Smith's lumped mass approach and the Method of Characteristics;
- The signal matching solution in general was shown to be non-unique; a reasonable match was obtained by three operators using different sets of parameters with the total capacity lying a maximum of 10% from the mean; in some cases significant differences in the interpreted mobilised shaft friction profiles were obtained;
- Correlation between static and dynamic tests must take into account any time effects on pile capacity, which were shown to be significant for the case presented;
- The correlation between tensile shaft capacity measured in static tests and the compressive shaft resistance measured in dynamic tests is critically dependent on the assumed split between internal and external shaft friction when interpreting DPT;
- The overall subjectivity of signal matching analyses, particularly when considering the mobilised shaft resistance profiles, has been highlighted along with the importance of verification of obtained capacity with static load tests.

9. Acknowledgements

This study is part of a JIP between Innovate UK, Iberdrola, Imperial College London and the Geotechnical Consulting Group. The Authors acknowledge Prof. Mark Randolph for the use of the IMPACT software and the support of Brian Mackenzie and Fugro

France for this work. The Authors also acknowledge Bilfinger Construction GmbH who carried out the offshore pile tests.

10. References

Barbosa P, Geduhn M, Jardine RJ, Schroeder FC and Horn M. (2015). Offshore pile load tests in chalk. *Proc. 16th Eur. Conf. Soil Mech. & Geotech. Eng,* Edinburgh, Scotland, pp. 2885-2890

Brucy F, Meunier J and Nauroy JF. (1991). Behavior of pile plug in sandy soils during and after driving. *Proc. Offshore Technology Conference*, Houston, Texas, pp. 145-154

Buckley RM, Jardine RJ, Kontoe S, Parker D and Schroeder, F. C. (2017a). Ageing and cyclic loading behaviour of piles driven in a low to medium density chalk. *Géotechnique.* In press.

Buckley RM, Jardine RJ, Kontoe S and Lehane BM. (2017b). Effective stress regime around a jacked steel pile during installation ageing and load testing in chalk. *Submitted to Can. Geotech. J.*

Byrne T, Doherty P, Gavin K and Overy R. (2012). Comparison of Pile Driveability Methods In North Sea Sand. *Proc. Offshore Site Investigation and Geotechnics (OSIG) Conf.*, London, UK, pp. 481-488

Chambers H and Lehane BM. (2011). An assessment of the geotechnical strength reduction factors specified in the new Australian piling standard. *Australian Geomechanics,* **46**, No. 4**,** 71.

Coyle HM and Gibson GC. (1970). Empirical damping constants for sands and clays. *J. Soil Mech. and F. - ASCE,* **96**, No. 3**,** 949-965.

Danziger BR, Lopes FR, Costa AM and Pacheco MP. (1996). A Discussion on the Uniqueness of CAPWAP–type Analysis. *Proc. 5th Intl Conf on the Application of Stress Wave Theory to Piles*, Orlando, Florida, pp. 11-13

Danziger BR, Costa AM, Lopes FR and Pacheco MP. (1999). Back analysis of offshore pile driving with an improved soil model. *Géotechnique,* **49**, No. 6**,** 777-799.

Dayal U and Allen JH. (1975). The effect of penetration rate on the strength of remolded clay and sand samples. *Can. Geotech. J,* **12**, No. 3**,** 336-348.

De Josselin De Jong G. (1956). Wat gebeurt er in de grond tijdens het heien. *De Ingenieur,* **68**, No.**,** B77-B88.

Deeks AJ and Randolph MF. (1995). A simple model for inelastic footing response to transient loading. *Int. J. Num. Meth. Geotech. Eng.,* **19**, No. 5**,** 307-329.

Fellenius BH. (1988). Variation of CAPWAP results as a function of the operator. *Proc. of the 3rd Int. Conf. on the Application of Stress Wave Theory to Piles*, Ottawa, Canada, pp. 814-825

Hannigan P, Goble GG, Likins G and Rausche F. (2006). *Design and Construction of Driven Pile Foundations,* Report No. FHWA NHI-05-042.

Holeyman A. (1985). Dynamic non-linear skin friction of piles. *Proc. Intl. Symp. on Penetrability and Driveability of Piles*, San Franscisco, California, pp. 173-176

Isaacs DV. (1931). Reinforced concrete pile formulae. *Paper No. 370, Trans. Aust. Inst. Eng.,* **XII**, No.**,** 321-323.

Jardine RJ, Chow FC, Overy R and Standing JR. 2005. *ICP design methods for driven piles in sands and clays,* London: Thomas Telford.

Litkouthi S and Poskitt TJ. (1980). Damping constants for pile driveability calculations. *Géotechnique,* **30**, No. 1**,** 77-86.

Middendorp P and Verbeek GEH. (2006). 30 Years of Experience with the Wave Equation Solution Based on the Method of Characteristics. *GeoCongress 2006*, pp. 1-6

Novak M, Aboul-Ella F and Nogami T. (1978). Dynamic soil reactions for plane strain case. *J. Eng. Mech. Div.,* **104**, No. EM4**,** 953-959.

Randolph MF and Simons HA. (1986). An improved soil model for one-dimensional pile driving analysis. *Proc. 3rd. Int. Conf. on Num. Meth. in Offshore Piling*, Nantes, France, pp. 3-17

Randolph MF. (2008). *IMPACT - Dynamic analysis of pile driving.,* Manual.

Rausche F, Goble GG and Likins Jr GE. (1985). Dynamic determination of pile capacity. *J. Geotech. Eng-ASCE,* **111**, No. 3**,** 367-383.

Rausche F, Robinson B and Liang L. (2000). Automatic signal matching with CAPWAP. *Proc. 6th Intl. Conf. on the Application of Stress-Wave Theory to Piles*, Sao Paulo, Brazil, pp. 53-58

Salgado R, Loukidis D, Abou-Jaoude G and Zhang Y. (2015). The role of soil stiffness non-linearity in 1D pile driving simulations. *Géotechnique,* **65**, No. 3**,** 169-187.

Smith EAL. (1962). Pile-driving analysis by the wave equation. *Geotechnical Special Publication,* **4**, No. 86**,** 35-61.

Svinkin MR. (2004). Some uncertainties in high-strain dynamic pile testing. *Proc. Geo Trans 2004*, Los Angeles, California, pp. 705-714

SYNTHETIC CPTS FROM INTELLIGENT GROUND MODELS BASED ON THE INTEGRATION OF GEOLOGY, GEOTECHNICS AND GEOPHYSICS AS A TOOL FOR CONCEPTUAL FOUNDATION DESIGN AND SOIL INVESTIGATION PLANNING

CF Forsberg, T Lunne and M Vanneste
Norwegian Geotechnical Institute, Oslo, Norway

L James
Forewind, UK/RPS, UK

TI Tjelta
Forewind, UK /Statoil, Norway

A Barwise
Statkraft UK Ltd. / RWE Innogy UK Ltd

C Duffy
Forewind, UK/Statkraft UK Ltd.

Abstract
Early phase soil investigation campaigns do not, as a rule, include all the locations where infrastructure is to be placed on the seafloor. However, background information on geology, bathymetric and seismic data may be available across the area at an early stage. The combination of these datasets provides the basis for developing a ground model of the development area. The inclusion of geotechnical data in such ground models is not always straightforward since geotechnical properties may vary laterally and with depth. In this paper we present an "Intelligent Ground Model", developed at NGI, and used at several large wind farm projects. The model combines interpreted seismic horizons with geological understanding and acquired CPTU data to allow synthetic CPTUs to be generated at any location within the investigated area. In the Dogger Bank wind farm area, synthetic CPTUs were generated at numerous locations to guide initial evaluations of foundation requirements and to group locations with similar synthetic profiles. The model was tested by removing known CPTU data from the database and comparing them to synthetic results from the same locations. The results show reasonably good matches.

1. Introduction

Offshore wind farms occupy large areas (tens to hundreds of square kilometres) in relatively shallow water (around 20 m). This means that the sites have been subjected to a variety of geological processes related to waxing and waning of ice age glaciers and changes in relative sea level and climate. A given location may for instance have experienced tundra-like conditions, subaerial exposure and shallow marine conditions during the course of the late Quaternary period. Heterogeneous properties of the seabed sediments should therefore be expected.

An offshore wind farm is often comprised of more than 100 turbines, each with an individual foundation. During the early conceptual phases or during a pre-bidding phase of wind farm development, it is unrealistic to have detailed geotechnical information from each of the turbine locations. We here present an automated method developed by The Norwegian Geotechnical Institute (NGI) for Forewind in connection with investigations of the Dogger Bank area. The method combines geophysical, geological and geotechnical information to produce synthetic CPTU (cone penetration testing with pore pressure measurements) profiles at any location within an investigation's boundaries.

2. Database

2.1 Prerequisites

The method does not run without initial human input. Some interpretations need to be performed ahead of running the scripts to establish the model database (Figure 1). The seismostratigraphy and its relation to geological units should be properly established. Each borehole / CPTU must be interpreted to identify if and at which depths the transitions in units occur. The input data thus consists of depth converted gridded seismic horizons (depth grids), a table with the depths at which geological units appear in each borehole/ CPTU and the CPTU data themselves. The bathymetry must exist as a separate grid.

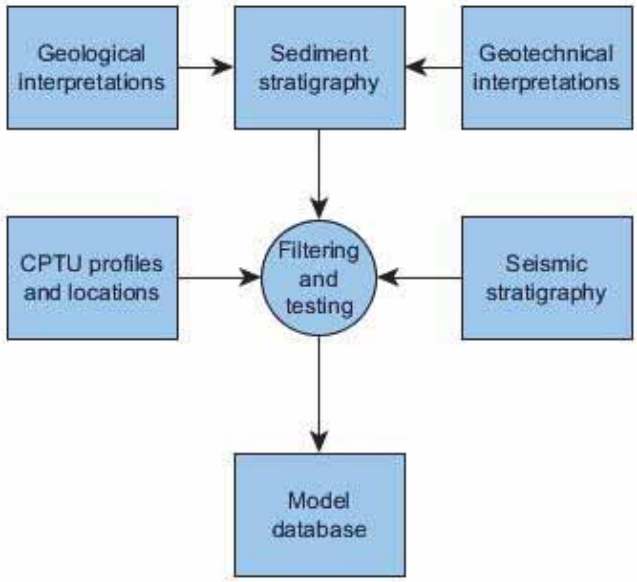

Figure 1. Inputs to synCPT database

2.2 Database construction

The database consists of a series of grids containing depths to the base of the layers identified in the boreholes/CPTUs and the corresponding parameters associated with each of these. Areas where units are absent are taken into account during the interpolation process by blanking the grids in such regions.

Interpreted seismic horizons guide the interpolation of the depths to the top and base of the units. If a unit boundary is not associated with a seismic horizon, the depths are guided by combining unit thickness variations with neighbouring units' boundaries.

2.3 CPTU interpretations

A prerequisite for the model database is that the sedimentary unit boundaries have been identified in the CPTU profiles. For each CPTU these boundaries must be given a depth or classified as not present or not penetrated. The latter indicates that the boundary is likely present below the penetration of the CPTU. Interpolation across a CPTU location where a layer is absent is not allowed whereas it is permitted where a boundary is not penetrated. A separate layer is automatically introduced for the first 2 m of penetration below the seafloor due to the differences in CPTU often seen in records from this interval compared to those deeper down due to low confining stresses.

The unit boundaries are used to associate different parts of the CPTU records with appropriate sedimentary units. The CPTU data within each of these sedimentary units are classified into smaller layers of either sand or clay according to whether they belong to one of the Robertson (1990; B_q vs Q_t) groups of four and above or below respectively. These subsets are separated in the database. Linear regression is applied to each of the two subsets in order to parameterise the curves. Thus, for each sediment unit in a CPTU, 13 different parameters are gleaned from the input curves:

- the relative content of sand and clay layers;
- the relative number of points within the sand layers with a q_t value above 20 MPa;
- the slope and intercept of the linear regression of the three data curves (q_t, B_q and F_r) for both sand and clay;
- the standard deviation of the q_t, B_q and F_r curve residuals after linearization;
- the depths to the top and base of each layer.

The application of several automated tests assures that spurious and erroneous results (e.g. spikes and initial part of CPTU strokes) are excluded from the data.

2.4 Interpolations

The parameters derived from the different CPTU sub-sections as described in the previous section are interpolated across the study area through minimum curvature gridding (*surface* program from the Generic Mapping Tools collection, Wessel et al., 2013) and later used for the construction of synthetic CPTUs. Values are removed from the grids in regions that are more than a maximum distance (set as an input parameter) from CPTU data and in areas where the seismic units associated with the sediment units being treated are absent. A grid is therefore produced for each of the parameters listed above. These grids are the main database for the program.

2.5 Interrogation of database

Synthetic CPTUs are constructed for a given location on a unit-by-unit basis. The top and bottom of the units are taken from the depth grids. CPTU profiles are constructed by calculating the appropriate parameters from the slope and intercept grids at the depths corresponding to the unit boundaries. Again, sand and clay parameters are calculated separately. While the database contains the relative content of sand and clay in a unit, it does not record the depths of sand and clay intervals within a given unit. The synthetic CPTU plot thus contains both sand and clay curves for mixed intervals, but only one of them where a single soil type is predicted to dominate. The relative content of sand and clay layers is, however, printed on synthetic output curves.